JOURNAL OF MATERIALS SCIENCE 28 (1993) 265–277

Microstructure and microanalysis of hardened ordinary Portland cement pastes

I. G. RICHARDSON, G. W. GROVES
Department of Materials, University of Oxford, Parks Road, Oxford OX1 3PH, UK

Hardened ordinary Portland cement pastes of various ages have been examined by analytical transmission electron microscopy (TEM) and electron microprobe analysis (EMPA). The stability of the various hydrate phases in the electron microscope is discussed. Although all are subject to damage in varying degrees, even the least stable phase, AFt, can be recognized in relict form in the TEM. The basic framework of the microstructure and the differentiation into inner and outer hydration product are well-established at 24 h hydration. Although the dominant inner product formed within the boundaries of the original anhydrous grains is C–S–H gel, particles of AFt, AFm, $Ca(OH)_2$, a magnesium-rich phase and an iron-rich phase are occasionally observed within the inner product. The Ca:Si ratio of the C–S–H gel determined by TEM shows significant variation from one region to another in a given paste. There is no relationship between the average Ca:Si ratio of the C–S–H and the maturity of the paste, although young pastes appear to show a bimodal distribution. Microanalysis by EMPA gives Ca:Si ratios in substantial agreement with those found by TEM but it is essentially impossible to obtain by EMPA analyses of outer product C–S–H without admixture of other phases, particularly sulphoaluminate phases. Despite the presence of small amounts of embedded phases as revealed by TEM, single-phase inner product C–S–H can be analysed by EMPA. The compositions of AFt and AFm phases have been obtained by TEM and the results do not require the substitution of silicon in the formulae.

1. Introduction

Electron microprobe analysis studies of flat and polished sections of hardened cement pastes have made valuable contributions to the compositional characterization of hydration products (for example, [1–3]). When used to "map" the surface, the technique can also provide spatial information. However, because the X-ray spatial resolution in bulk specimens is poor, unseen inhomogeneities may contribute to the analyses and so mislead the interpretation. In thin specimens the X-ray resolution is of the order of the probe size; this enables the identification and analysis in the transmission electron microscope (TEM) of features on a significantly sub-micrometre scale. Unfortunately, the complex multiphase nature of hydrated cements makes the preparation of thin specimens for TEM examination far from trivial, which is why until recently all TEM studies had been of synthetic hydration products or of ground and dispersed cement pastes [4–7]. Groves and co-workers [8–10] have successfully achieved the thinning of hardened cement pastes by the use of ion-beam milling, and by using a liquid-nitrogen-cooled cold stage to minimize thermal damage. This technique was adopted in the present work. This is a long process, often taking days rather than hours and the possibility of developing artefacts during the preparation must be considered. Clearly, the drying effect of the vacuum of the ion-beam thinning apparatus and carbon evaporation chamber is unavoidable, but as the microscope also operates at high vacuum it must be accepted that any observed morphologies correspond to a dry state. The possibility of thermal damage during preparation is potentially more serious than if it occurred during observation in the microscope, as in the latter case the operator would probably have observed its effects. It is therefore essential to employ thinning rates of $< 4\ \mu m\ h^{-1}$ and to use a cooled stage. Rodger and Groves [11] examined a mature ordinary Portland cement (OPC) paste using TEM with microanalysis, identifying many of the main features, but they did not attempt to address the apparently contradictory results reported in the literature for the compositions of the main hydration products (comprehensively discussed by Taylor [12]). This paper presents such a study.

2. Experimental procedure

2.1. Materials

A single batch of a Blue Circle (Northfleet) ordinary Portland cement was used throughout this work. Its oxide composition is shown in Table I. The tricalcium silicate (C_3S) used in this work was prepared by the method used by Groves *et al.* [8].

0022–2461

TABLE I Oxide composition (wt %) supplied with the Blue Circle Northfleet OPC

Na_2O	0.19	K_2O	0.86
MgO	1.33	CaO	65.90
Al_2O_3	6.19	TiO_2	0.30
SiO_2	20.00	Mn_2O_3	0.06
SO_3	2.65	Fe_2O_3	3.03

2.2. Sample preparation

The samples were prepared by mixing the required amounts of solids with de-ionized water at a water to solids ratio of 0.4. The resulting slurry was placed in plastic tubes which were then sealed in plastic bags before placing in cure baths set at 20 °C. Samples were removed from the cure baths at pre-determined times. For thermal analysis they were crushed, washed in propan-2-ol, filtered, and stored in a vacuum desiccator prior to analysis. The specimen preparation techniques for electron microscopy are given below.

2.3. Electron microprobe analysis

The X-ray analysis of a bulk specimen was performed on a Cameca Camebax electron microprobe equipped with one energy dispersive (EDS) and two wavelength dispersive (WDS) detectors. Sections 2 mm long were cut from the cylinder of a 2 year old hydrated OPC and submerged in propan-2-ol before placing in a vacuum desiccator. One of the "dried" specimens was carefully polished down. Great care was taken to minimize preferential polishing of the hydrated phases; a flat, polished surface is essential for quantitative analysis as surface irregularities affect the matrix correction factors.

The microprobe was operated at an accelerating voltage of 15 kV and probe current of 3×10^{-8} A. Charging effects were minimized by the application of a thin coating of carbon after the specimen had been polished. The X-ray mapping involved the simultaneous analysis of ten elements (Na, Mg, Al, Si, S, K, Ca, Ti, Mn and Fe) for a total of 2500 analyses (50×50 square; 1 μm increments). Iron and sodium were analysed with the WDS detectors and the remaining eight by the EDS detector. Full ZAF corrections were applied on the University VAX computer. Oxygen was calculated by the difference. This produced incorrect absolute atom fractions but correct atom ratios.

2.4. Transmission electron microscopy

The specimens were polished down to 30 μm thickness and glued between 3 mm diameter nickel grids which had 2 mm × 1 mm central holes through which the sandwiched sample was exposed. They were then argon ion-beam milled until the centre of the exposed samples had thinned to a hole. Much of an approximately 10 μm deep region around the holes was generally electron transparent. Thinning was at rates of $< 4\ \mu m\ h^{-1}$ and included the use of a cooled stage to help minimize thermal damage. The specimens were carbon coated in a high-vacuum evaporation chamber. The samples were examined in a Jeol 2000FX transmission electron microscope equipped with a Tracor Northern TN5500 X-ray microanalysis facility. The EDS detector (beryllium window) had a high take-off angle which enabled analyses to be performed without tilting the specimen. This facilitated the collection of statistically relevant sets of data. The microscope was operated at 200 kV.

In general, quantitative analysis of thin specimens can be achieved without recourse to complex correction procedures; if the specimen is thin enough then absorbtion becomes negligible [13], and the analyses need only be corrected for the efficiency of collection. However, complications can arise when two or more elements of interest have very close K_α lines. This problem was encountered in this work where magnesium, aluminium and silicon were often simultaneously present. The main effect was an underestimation of the aluminium content. An empirical correction factor, which was derived to compensate for this, was found to be effective in improving the data over most of the compositions encountered. The standards used to derive the (K-ratio) factors to correct for the efficiency of collection included Åkermanite ($Ca_2MgSi_2O_7$), Wollastonite ($CaSiO_3$), C_3A ($Ca_3Al_2O_6$), anhydrite ($CaSO_4$), K_2SO_4 and C_4AF.

3. Results and discussion

3.1. Microstructure

3.1.1. Reference structure

During the hydration of tricalcium silicate, $Ca(OH)_2$ and two distinct calcium silicate hydrate gels are formed [8, 9]. These C–S–H phases are designated as being either "inner" (Ip) or "outer" (Op) product. Inner product C–S–H forms within the boundary of the original particles and outer product C–S–H forms in originally water-filled space. Calcium hydroxide also forms in the outer product region. As the silicate phases alite (impure C_3S) and belite (impute β-C_2S) are the most abundant minerals in OPC, this scheme serves as a convenient reference structure for OPC-based hardened cement pastes.

3.1.2. Stability of hydration products in the TEM

Many of the phases commonly present in hardened cement pastes suffer thermal and irradiation damage during preparation and observation in the TEM. Because the morphologies of all the common hydration products occurring in hardened OPC pastes are considered in this paper, it is important to emphasize the use of standardized conditions of sample preparation and examination. Table II lists many of these phases and their relative stabilities when viewed under standard conditions in the TEM. These conditions, which are given at the bottom of the table, correspond to those established as being most satisfactory for the *rapid* viewing of a hydrated Portland cement. It must be emphasized that for a more lingering examination a

TABLE II Relative stability of hydration products during observation in TEM under standard conditions[a]

Phase	Approximate composition	Decomposition temperature (°C)	Stability 0 1
Calcium silicate hydrate gel	C–S–H variable	$pk \approx 130$ $100 \rightarrow 320$	
Outer product hydrate gel in OPC or C_3S	$C_{1.7}SH_a$	$pk \approx 125$ $100 \rightarrow 320$	
Inner product hydrate gel in OPC or C_3S	$C_{1.7}SH_b$	$pk \approx 125$ $100 \rightarrow 320$	
Outer product hydrate gel in GGBFS/5M KOH	$C_{1.1}SH_c$	$pk \approx 145$ $100 \rightarrow 350$	
Calcium hydroxide	$Ca(OH)_2$	$490 \rightarrow 540$	
Ettringite	Impure $Ca_3Al_2O_6 \cdot 3CaSO_4 \cdot 32H_2O$	$106 \rightarrow 136$	
AFm	$[Ca_2(Al, Fe)(OH)_6] \cdot X \cdot yH_2O$ $X = OH, CO_3, SO_4$, etc.	$180 \rightarrow 205$	
Monosulphoaluminate hydrate	$Ca_3Al_2O_6 \cdot CaSO_4 \cdot 12H_2O$	200	
Mg-rich phase (hydrotalcite related)	$Mg_{1-x}Al_x(OH)_2R^{-n}_{x/n} \cdot yH_2O$ $0.20 < x < 0.33$ $R = OH, CO_3, SO_4$, etc.	≈ 250	
Gehlenite hydrate	$Ca_2Al_2SiO_7 \cdot 8H_2O$	180	

[a] Accelerating voltage 200 kV; LaB_6 filament; medium–large spot size (2); medium condenser aperture (about 50 μm); medium objective aperture; magnification ×21 000; beam defocused to two-thirds the limit of the field of view.

smaller spot size and greater beam defocus are essential. The stability is defined as being the relative dwell time that a phase can endure in the centre of the field of view before noticeable damage occurs. The scale is set for convenience from 0–1, and the relative positions would probably not vary much between microscopes operated under similar conditions (and by the same operator as this is based on observational judgement). 0 corresponds to instantaneous damage on moving into the field of view, as is indeed occasionally observed; however, most phases this susceptible would generally already have suffered extensive damage during preparation, for example AFt phases. 1 is less easy to define quantitatively, but in this work probably corresponded to a dwell time of around 60 s. The lighter shading is used where a phase can display marked variation. Peak decomposition temperatures, as recorded using DSC, are also listed in the table for the purpose of comparison with the relative stabilities. As the table indicates, in a neat OPC paste the Ip C–S–H is less stable than the Op C–S–H. In practice, this manifests itself as a coarsening of the C–S–H structure. This is illustrated in Fig. 1a and 1b. These micrographs are of an inner product region in a mature hardened Portland cement paste (20 °C; W/C = 0.5). The lath-like features in the centre of the micrographs are probably a C_4AH_x type phase. The presence of phases other than C–S–H within the inner product region is considered later. Fig. 1a was taken soon after bringing the area into the field of view. The C–S–H has a compact, homogeneous, fine-scale structure. On further observation under "standard conditions" (see Table II), the structure rapidly coarsened, the micrograph in Fig. 1b being taken only around 15 s after the first exposure. The amount of damage suffered in this very short time is sharply evident. It must also be noted that the structure in Fig. 1a may be coarser than in an undisturbed hydrating paste, as TEM samples undergo partial dehydration during preparation. The use of a cold stage during ion-beam milling is essential for hardened OPC pastes to minimize thermal damage. When considering whether the morphology of C–S–H just brought into the field of view may have sustained avoidable damage, one must not only consider the sample preparation technique or whether the area has been previously examined, but also how the beam had been manipulated over the specimen. For example, damage can occur over an extensive area if the beam current is initially turned up at low magnification with a large spot size and poorly defocused electron beam.

3.1.3. *Microstructure after 24 h hydration and its development on further reaction*

It is inherent in the ion-beam milling technique that the sample is sufficiently coherent to allow thinning without large areas simply dropping out. As a consequence the youngest pastes to be thinned over a large enough area to hopefully be a reasonable representation of the bulk specimen (and to allow as statistically significant a number of X-ray analyses as possible to be made of both Ip and Op C–S–H) had been hydrated for 24 h (20 °C; W/C = 0.4). The microstructure of younger samples is at present best studied by the secondary electron imaging (SEI) of fracture surfaces. The difficulty in preparing TEM specimens of young pastes, and problems associated with other electron microscopy techniques, renders the direct acquisition of reliable compositional information on early-stage hydrates almost impossible on a routine basis with the instrumentation currently available. However, the resin impregnation of samples, as adopted by

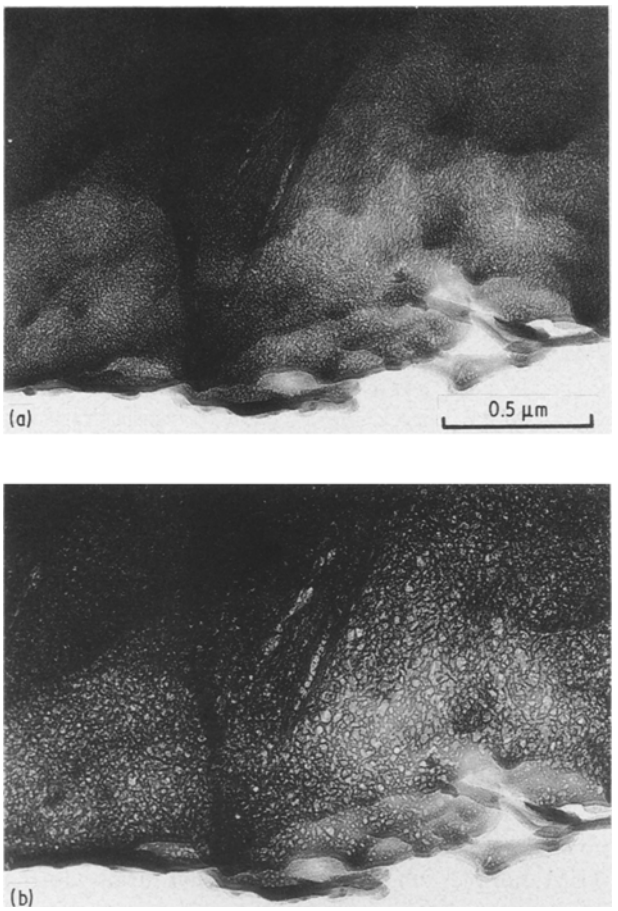

Figure 1 Transmission electron micrographs of an inner product region in a mature hardened Portland cement paste taken (a) soon after bringing the area into the field of view, and (b) ≈ 15 s after the first exposure.

Dalgleish and co-workers [14, 15] may go some way towards overcoming these obstacles.

A substantial degree of reaction is achieved during the first 24 h hydration (at normal temperatures and W/C ratios) and the reference microstructure is already well-established by this time. However, the outer product region is still very open and is often occupied by large quantities of AFt crystals, which are highly hydrated and readily decompose during sample preparation. These points render the production of TEM specimens difficult, and the resulting microstructure "messy" for TEM examination. Nevertheless, large areas of both coarse and fine fibrillar Op C–S–H are often observed, as are extensive regions of Ip C–S–H with the familiar homogeneous fine-scale morphology. $Ca(OH)_2$ crystals are a common feature in the outer product region and are, as in C_3S pastes, often well-bonded with fine-fibrillar Op C–S–H. Although considerable further reaction and microstructural development occurs after ≈ 24 h, and at a slower rate, the main microstructural features are maintained. These features gradually develop as reaction proceeds: the outer product regions between the original cement grains continue to fill in with C–S–H gel and calcium hydroxide; areas of Ip C–S–H extend as the larger alite grains continue, and the belite starts to react; large plates of AFm form at the expense of AFt, although AFt may sometimes persist indefinitely.

3.1.4. Hydrated phases within the outer product region

The outer product region contains four major phases; C–S–H gel, $Ca(OH)_2$, AFm and AFt. Of these, the C–S–H gel and $Ca(OH)_2$ are by far the most abundant. As in C_3S pastes, the morphology of Op C–S–H seems to be a function of space constraint: where it forms in large pore spaces, it exhibits a fibrillar, directional character, with a high aspect ratio; in smaller spaces, it retains a directional aspect but forms in a more space-efficient manner. Again as in hardened C_3S pastes, calcium hydroxide typically occurs in the outer product as massive crystals, often many micrometres in length. Bonding with Op C–S–H is generally excellent, except when the interface is parallel to the basal plane of the $Ca(OH)_2$. In such circumstances, as in C_3S pastes, a thin layer of C–S–H forms along the crystal surface parallel to the basal plane, and the bulk fine-fibrillar C–S–H is bonded to this.

The high (AFt) and low (AFm) sulphate-bearing aluminate hydrate phases vary in relative abundance depending upon the degree of hydration, the (aluminate + aluminoferrite): sulphate ratio, the form of the sulphate in the cement, and many other factors. AFm is present in mature pastes as large irregular plates which on appearance alone can easily be mistaken for $Ca(OH)_2$, although they are more unstable in the

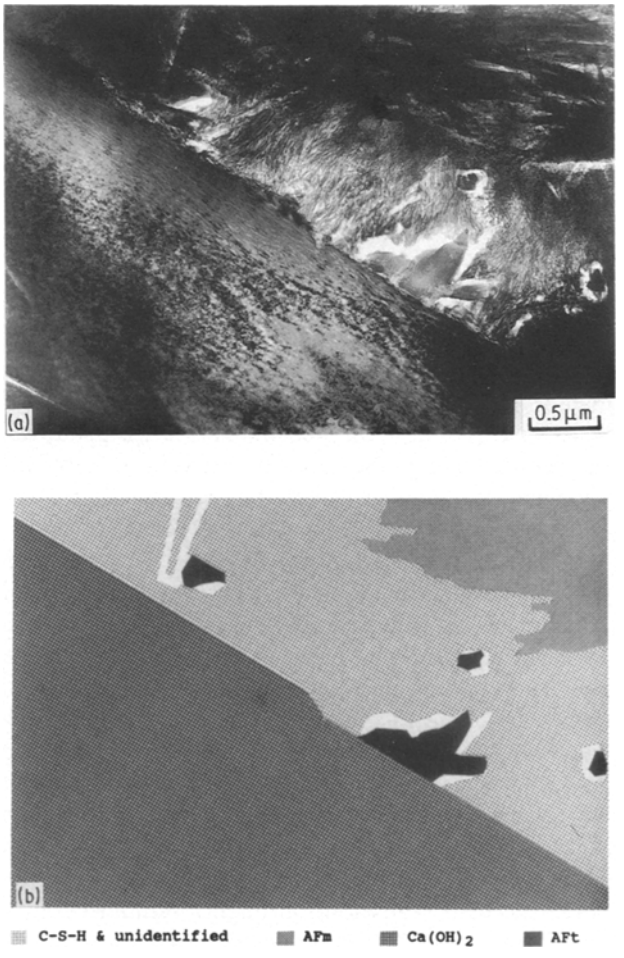

Figure 2(a) Transmission electron micrograph and (b) schematic diagram showing $Ca(OH)_2$, fine fibrillar C–S–H, AFm plates and AFt relicts in the outer product region of a paste hydrated for 3 months (W/C = 0.4, 20 °C).

TEM and rapidly lose crystallinity. Aft occurs as thin hexagonal prism needles, up to 10 μm long. Both phases are present in Fig. 2a. Their positions are indicated on the schematic diagram accompanying the micrograph (Fig. 2b). EDXA confirmed the plate-like crystals to be a low-sulphur AFm. The two small features are cross-sections through AFt needles (the composition was confirmed by EDXA to be that of AFt). It would appear that the AFt crystals had shrunk during sample preparation leaving relicts and an outline in the C–S–H of their original shapes. In some areas the hexagonal nature of AFt can be seen in the impressions left in the surrounding C–S–H.

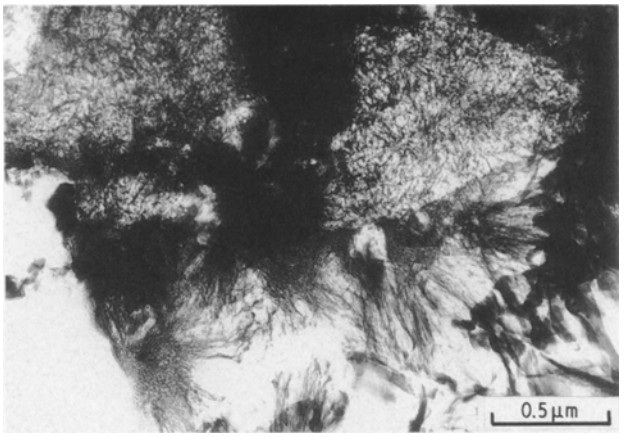

Figure 3 Transmission electron micrograph showing small, fully hydrated grains with coarse, foil-like Ip C–S–H, in a paste hydrated for 3 months (W/C = 0.4, 20 °C).

3.1.5. Hydrated phases within the inner product region

Inner product regions in mature OPC pastes most commonly consist of single-phase C–S–H, which has the same compact, fine-scale and homogeneous morphology as the Ip C–S–H present in hardened C_3S pastes. Another characteristic of C_3S pastes, is the presence of small hydrated grains with an unusually coarse Ip C–S–H containing substantial porosity, and surrounded by a zone of relatively dense C–S–H. Indeed, this appears to be a feature of small hydrated particles in general, whether of C_3S, in OPC, or of slag particles or fuel-ash particles in a blended paste [16]. This feature may have implications for the design of low-permeability cements. Examples of these grains occurring in an OPC paste are shown in Fig. 3. Although the Ip C–S–H in these grains tends to have a lower than average Ca:Si atom ratio (i.e. < 1.75), it is by no means a rule, as this example shows; the right-hand grain has a Ca:Si ratio of 1.58 and the left-hand grain a ratio of 1.80. The Op C–S–H close to the left-hand grain has a ratio of 1.81, which is similar to that of the Ip C–S–H. The similarity between the Ca:Si ratio of Ip C–S–H and adjacent Op C–S–H is a common observation.

The bonding between Ip and Op C–S–H is generally excellent, with an often poorly defined interface. This is illustrated in Fig. 4a, a transmission electron micrograph with both inner and outer product regions, and Fig. 4b, a schematic representation of the area. The interface in the top left-hand quarter appears at first glance to be well defined, but on examination the Ip C–S–H seems to extend some hundreds of nanometres past the boundary. The interface on the right-hand side of the micrograph is even more confused, and interpretation is hindered by the presence of AFt relicts within the interface region. A problem in defining the interface is that the Op C–S–H tends to radiate into the outer product region in a fan-like manner from relatively small areas. The C–S–H at these points of "nucleation" thus tends to be fairly dense and apparently without directionality, rendering it morphologically indistinguishable from the Ip C–S–H. This "blurring" region may extend over several hundred nanometres.

Although C–S–H was the most abundant inner product hydrate, a common characteristic of the OPC pastes examined during this study was the presence of phases other than C–S–H within the inner product region. These included all the major phases (i.e. AFt, AFm, $Ca(OH)_2$) and some minor phases (magnesium- and iron-rich phases). Evidence for the presence of AFt has already been noted with Fig. 4, and was observed as early as 7 days. However, clusters of AFt within the inner product have also occasionally been observed, but only in the more mature pastes ($\approx$ 12 months). Thinning often sections the AFt needles, the damaged relicts leaving a roughly hexagonal impression in the surrounding C–S–H, whether inner or outer product (an example in the Op C–S–H is shown in the top right-hand corner of Fig. 4a). When thinning occurs along the length of the needle, the AFt relicts appear as in Fig. 5. The AFt relicts run down the middle of the features, leaving impressions of their undamaged shapes. If the C–S–H around a more stable phase damaged during preparation or under the influence of the electron beam, then this second phase may remain intact; however, if C–S–H containing the impressions of an already damaged phase were to coarsen, this would then also affect the relict. This fact would seem to suggest that the observed Ip C–S–H morphology, although in a "dried" state, is a good representation of its true structure.

A third phase, more stable than the AFt, is also present in Fig. 5 (in the top right-hand corner). This particular crystal is a magnesium-rich phase, but from appearance and stability alone it could easily be taken to be of the AFm family, crystals of which have also been observed in this study to occur within the inner product region. Fig. 6 shows a large region of Ip C–S–H which possesses several of the magnesium-rich crystals. The formation of such phases within Ip C–S–H implies a through-solution mechanism for the formation of inner product.

Calcium hydroxide is generally associated with outer product regions. Fig. 7 shows the interface between Ip C–S–H and a crystal of $Ca(OH)_2$ growing in the outer product region. The bond appears to be very good. It was stated earlier that $Ca(OH)_2$ has been observed in this study intermixed with Ip C–S–H. Indeed, it has been observed in samples ranging from

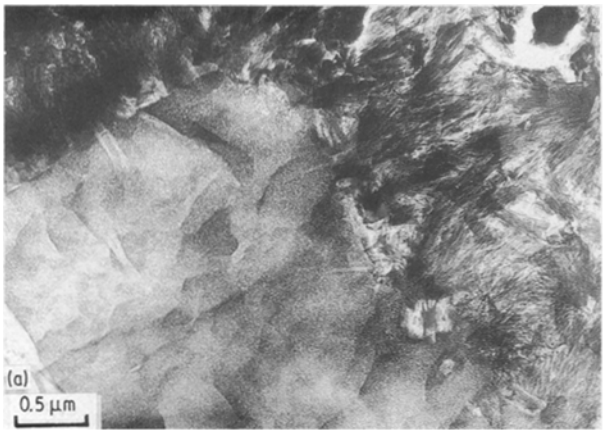

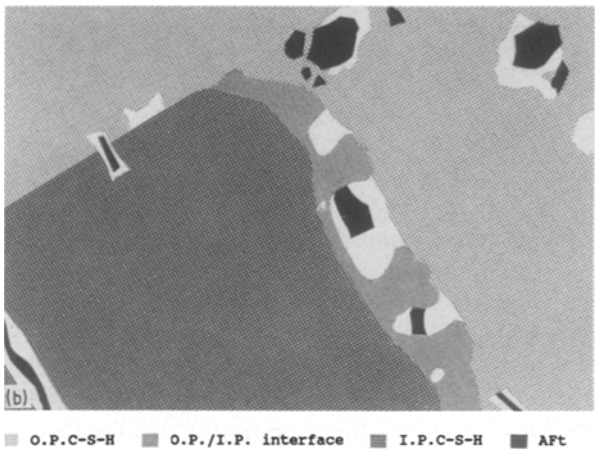

Figure 4(a) Transmission electron micrograph and (b) schematic diagram showing an inner/outer product interface region in a paste hydrated for 3 months (W/C = 0.4, 20 °C).

Figure 5 Transmission electron micrograph showing AFt relicts in a large inner product region in a mature OPC paste.

24 h–3½ years old. It is probably not a major feature of inner product regions, but is common enough to be easily found in a standard TEM specimen. It also occurs over a range of dimensions; from quite small, as in Fig. 8, to several micrometres. It is notable that the C–S–H adjacent to $Ca(OH)_2$ nearly always has a Ca:Si ratio greater than the mean value (i.e. > 1.75). As a result of the care taken in these measurements, it is unlikely that the $Ca(OH)_2$ itself made any significant

Figure 6 Transmission electron micrograph showing Mg, Al-rich laths in a large inner product region in a mature OPC paste.

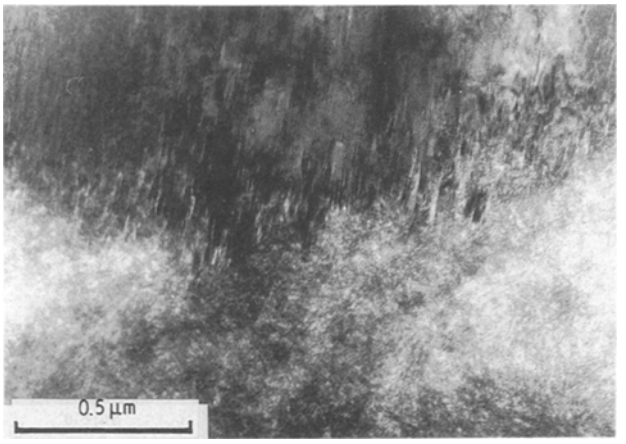

Figure 7 Transmission electron micrograph showing an interface between a $Ca(OH)_2$ crystal in the outer product, and inner product C–S–H.

contribution to the analyses (the $Ca(OH)_2$ was identified by EDXA and electron diffraction).

3.2. Microanalysis

3.2.1. Chemical composition of C–S–H gel: TEM results

Table III shows the mean Ca:Si ratios of both Ip and Op C–S–H in hardened OPC pastes of between 1 day and 3½ years age (20 °C; W/C = 0.4). All analysed regions appeared on visual examination to be single-phase C–S–H but were checked by selected-area diffraction to ensure the absence of crystalline phases.

All analysed inner product regions were from different grains except in Sample 1 year[1], which were all from one large grain. Before comparing the results at different ages, it is worthwhile first considering the 1 year old samples. Six TEM specimens were examined for this age. On inspection it is evident that there is significant variability in mean Ca:Si ratio. In all cases the ratio for the Ip C–S–H is higher than that for the Op C–S–H, with the standard deviation lower in all but one sample for the outer product. The difference between the values for the two regions is also variable, e.g. narrower in Samples 2 and 3 than in Sample 5.

Figure 8 Transmission electron micrograph showing small $Ca(OH)_2$ crystals embedded in inner product C–S–H.

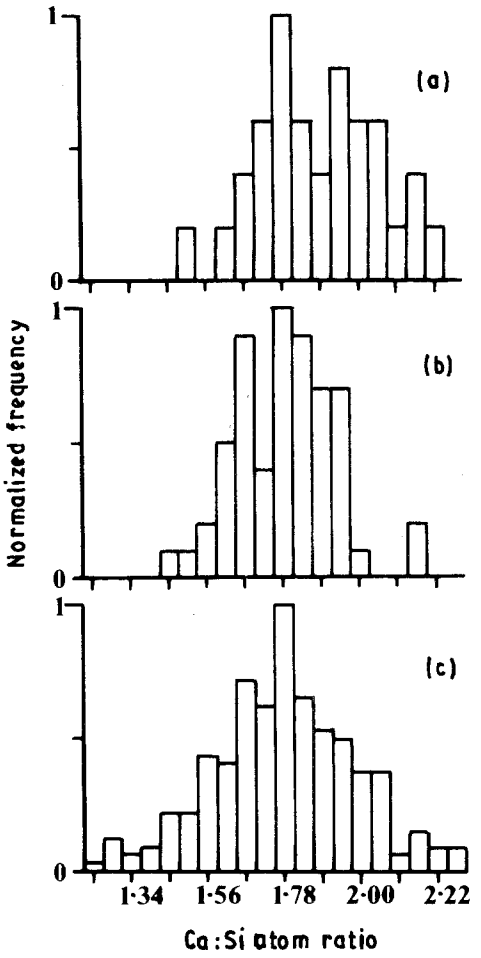

Figure 9 Ca:Si atom ratio frequency histograms for both Ip and Op C–S–H present in the 1 year old pastes in Table III, (a) Sample 1, (b) Sample 4, and (c) the combined data of Samples 1, 3, 4, 5 and 6.

TABLE III Ca:Si atom ratios in hardened OPC pastes. W/C = 0.4, 20 °C

	Inner C–S–H		Outer C–S–H	
	$x \pm \sigma$	(*n*)	$x \pm \sigma$	(*n*)
1 day	1.86 ± 0.21	(21)	1.57 ± 0.25	(12)
1 week	1.65 ± 0.21	(27)	1.69 ± 0.16	(24)
3 months	1.73 ± 0.15	(19)	1.73 ± 0.13	(20)
1 year[1]	1.90 ± 0.17	(27)	1.72 ± 0.07	(4)
1 year[2]	1.65 ± 0.17	(15)	1.61 ± 0.16	(14)
1 year[3]	1.80 ± 0.17	(31)	1.76 ± 0.12	(27)
1 year[4]	1.84 ± 0.19	(28)	1.75 ± 0.12	(31)
1 year[5]	1.87 ± 0.17	(14)	1.62 ± 0.14	(12)
1 year[6]	1.77 ± 0.14	(15)	1.61 ± 0.22	(12)
2 years	1.89 ± 0.12	(21)	1.87 ± 0.08	(22)
$3\frac{1}{2}$ years	1.75 ± 0.15	(26)	1.74 ± 0.10	(25)

Rayment and co-workers [1, 17] have reported analyses of C–S–H in hardened cement pastes displaying a bimodal Ca:Si ratio distribution. This characteristic is prevalent in many of the present samples. Fig. 9a and b show the frequency distributions for Samples 1 and 4, respectively. Fig. 9b illustrates the wide variation in composition for both Op C–S–H and Ip C–S–H from different grains. As all inner product analyses in Sample 1 were from the same grain, Fig. 9a indicates that the variation is also intra-grain. Fig. 9c shows the normalized frequency curve for the combined data of Samples 1, 3, 4, 5 and 6, that is, from different regions of the 1 year old sample, in which a bimodal distribution is not evident. This could be interpreted as being due to summing distributions which are themselves bimodal but at slightly different Ca:Si ratios. This interpretation is supported by considering analyses of mature hardened C_3S pastes (Fig. 10) and older OPC data, Fig. 11e (2 years), which have similar statistics but display no pronounced bimodularity, and also, younger OPC data which do display bimodal characteristics, Fig. 11a–d. All analyses were performed using the same standardized technique, so it seems most probable that the steady trend of increasing bimodularity with decreasing age is a real feature. This observation is consistent with the view that C–S–H tends towards a compositional equilibrium, and the idea that C–S–H is composed of an intimate mix of calcium silicate compositional units whose Ca:Si ratio can vary with silicate chain length [7, 18, 19]. The mean Ca:Si ratio values for the 1 week, 3 months, 2 and $3\frac{1}{2}$ year old OPC pastes all have very similar values for both Ip and Op C–S–H, although the ratio is generally lower in the outer product, which also has a smaller standard deviation. There is no relationship between Ca:Si ratio and maturity of paste, so any differences would seem to be due to compositional variability within the paste. This is reflected in the variability evident between the 1 year old samples.

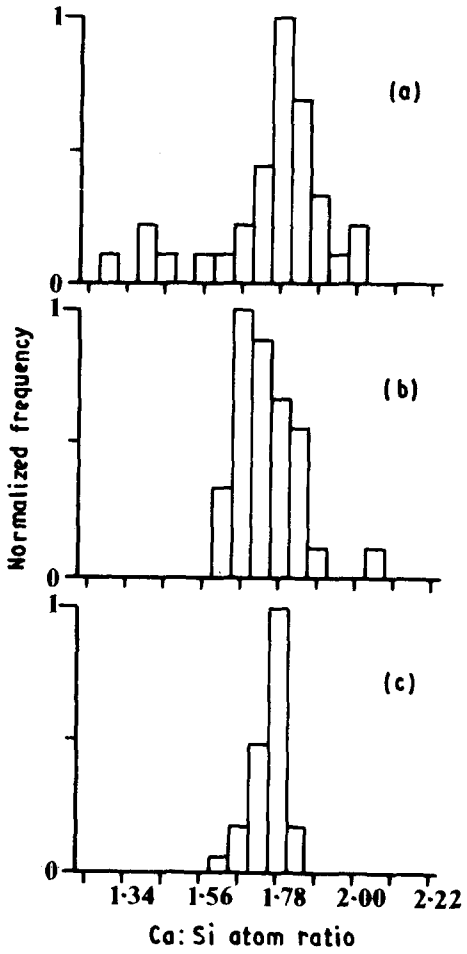

Figure 10 Ca:Si atom ratio frequency histograms for C–S–H in hardened tricalcium silicate pastes. (a) $3\frac{1}{2}$ years, Op C–S–H, $n = 32$; (b) $3\frac{1}{2}$ years, Ip C–S–H, $n = 33$; (c) 26 years, Ip C–S–H, $n = 31$.

The C–S–H present in OPC pastes may contain small amounts of minor elements. Aluminium is generally considered the most significant substituent. Unfortunately, the restraints placed on the EDXA technique by the beam-sensitive nature of C–S–H gel and the close proximity of AlK_α and SiK_α lines, causes problems in establishing the true levels of aluminium in C–S–H phases.

It is notable that only a small fraction of the total number of analyses collected for each paste recorded the presence of aluminium. Clearly the mean of all values would be dramatically reduced if all the other analyses were taken as having zero aluminium. However, aluminium was often observed on the EDXA spectrum when it had not been detected by the peak stripping program (generally because of interference from the silicon peak and not through lack of statistics). As an indication of the true mean Al:Ca ratio, for a set of data for both the 1 and 2 year old pastes, such analyses were recorded and were given a value equal to $\{(0.147\,07 \times \text{Mg}) + (0.076\,03 \times \text{Si})\}$. This was derived by outputting the unprocessed counts from each energy channel contributing to the K_α peaks of magnesium, aluminium, silicon and calcium, subtracting an estimated level for background counts, summing the channels for each peak, and then comparing this value with the program-derived integrated value. This process was repeated for two analyses with different Mg:Al ratios. The results of the manual processing

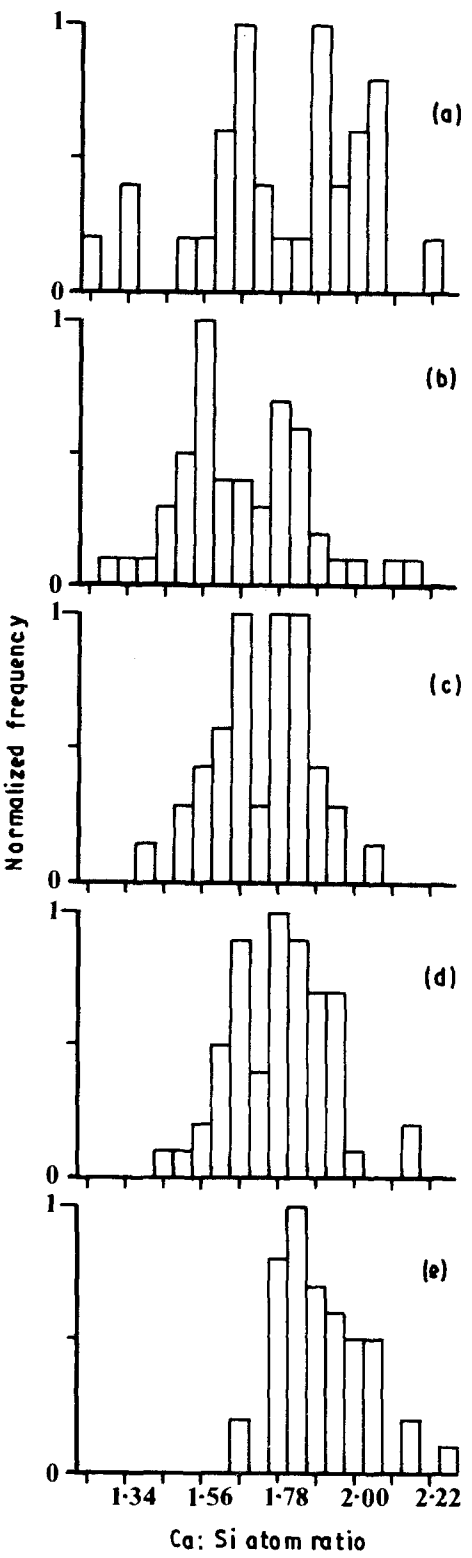

Figure 11 Ca:Si atom ratio frequency histograms for both Ip and Op C–S–H present in OPC pastes hydrated for various times. (a) 1 day, $n = 32$; (b) 1 week, $n = 51$; (c) 3 months, $n = 39$; (d) 1 year, $n = 58$; (e) 2 years, $n = 46$.

were within 2% of the program-derived values for magnesium, silicon and calcium but $\approx 100\%$ greater for aluminium. The contributions from magnesium and silicon in reducing the program-derived aluminium count (by peak overlaps) were then calculated by simultaneous equations to give the relationship for the corrected aluminium count

$$\text{Corrected Al} = [\text{Al} + (0.147\,07 \times \text{Mg}) + (0.076\,03 \times \text{Si})] \quad (1)$$

This simple correction is effective in improving the aluminium counts so that there is good agreement between TEM and EMPA data; this is more effectively demonstrated in another paper [20]. The correction is only valid, however, over a fairly restricted range of composition and using the short analysis times (and therefore low total counts) imposed by the poor stability of the hydration products.

The results of applying this correction to the mature OPC pastes mentioned, are summarized in Table IV. The mean Al:Ca ratios of the analyses detected by the program give the impression that aluminium is present in Ip and Op C–S–H in similar quantities, but it is apparent from the difference in the number of analyses where aluminium was detected (Table IV) that this may not be the case, and that the Op C–S–H may have a higher mean Al:Ca ratio.

All the TEM analyses of C–S–H are regarded as having been of single-phase C–S–H, with the presence of other phases excluded. The presence of second phases on a fine, but observable scale, has also been demonstrated. If the detected levels of aluminium were due to the intimate mixing of AFm-type layers with calcium silicate layers within the C–S–H on a scale too fine to be distinguished, then the Al:Ca ratio would increase with increasing Ca:Si ratio. Equally, if one gradually replaced the silicon with aluminium in a C–S–H of fixed Ca:Si ratio, then the Al:Ca ratio would also increase as the Ca:Si ratio increased. However, if one imagines a series of C–S–H phases with a range of Ca:Si ratios, then the replacement of the same fraction of silicon atoms with aluminium in each phase would result in a series where the Al:Ca ratio increased as the Ca:Si ratio reduced. This is the observed trend for the C–S–H in mature neat OPC pastes, Fig. 12, and for the Op C–S–H in hardened blast-furnace slag/OPC blends (slag fraction 0–1) [20], and indicates that the aluminium is indeed probably replacing a fraction of the silicon in the C–S–H gel. This is considered later with respect to EMPA bulk analyses. Other minor elements regularly detected within both Ip and Op C–S–H include iron and sulphur. Neither the Fe:Ca or S:Ca ratios displayed any discernable relationship with the Ca:Si ratio of the C–S–H, though they both showed a slight tendency to decrease with increasing calcium counts. This is associated with the very low X-ray counts involved with the minor elements.

Although this renders quantification of the data difficult, it is notable that the samples with the highest

TABLE IV Al:Ca atom ratios in hardened OPC pastes. W/C = 0.4, 20 °C

	Inner C–S–H		Outer C–S–H	
	$x \pm \sigma$	% tot	$x \pm \sigma$	% tot
Al detected by program only	0.076 ± 0.012	14	0.082 ± 0.012	43
Al detected by program and visually	0.062 ± 0.012	54	0.075 ± 0.015	69
All analyses	0.033 ± 0.032	100	0.052 ± 0.037	100

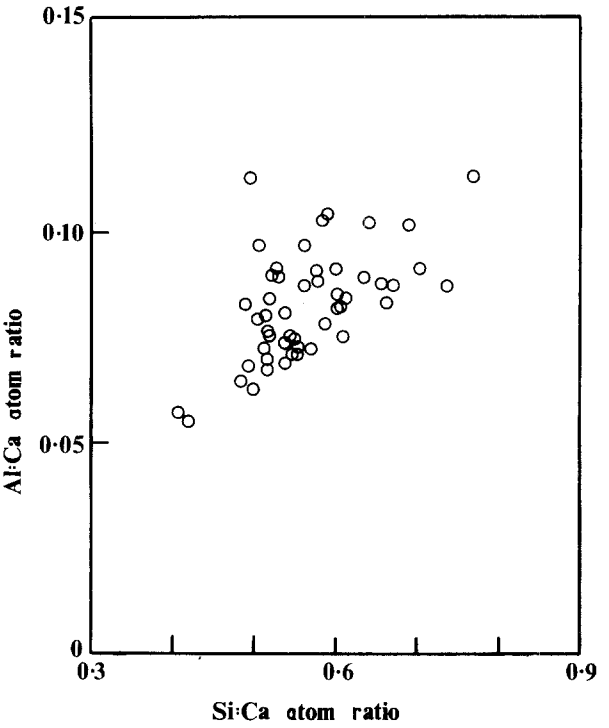

Figure 12 Al:Ca atom ratio against Si:Ca atom ratio for C–S–H in hardened OPC pastes.

number of analyses detecting iron or sulphur as a proportion of the total number, are not the same for the two elements. Although, as for aluminium, the presence of these elements was sometimes observed on the spectrum when not detected by the peak stripping program, unlike for aluminium this was due to poor statistics and so it was not possible to make any empirically determined correction. A characteristic of Ip C–S–H is its retention of magnesium. On *no* occasion was magnesium ever detected by TEM in the outer product region of hardened OPC pastes.

3.2.2. Chemical composition of C–S–H gel: microprobe results

Bulk compositional information was obtained for a mature hardened OPC paste by the EMPA mapping technique. As both inner and outer regions are of interest, the area chosen for analysis was centred around a partially reacted alite grain. An examination of the elemental maps, especially a comparison between those of magnesium and Ca:Si ratio, noting that magnesium was not detected in the outer product region by TEM, readily reveals the Ip C–S–H regions. The magnesium originally present in the anhydrous alite, as suggested by Taylor and Newbury [2], does not migrate away from the inner product region during hydration, and as such can be regarded as a chemical marker for the boundary of the original grain.

The criteria used to determine which analyses corresponded to inner and outer product C–S–H were as follows.

1. After the subtraction of empirically determined noise levels, Ip C–S–H was regarded as having Mg > 0 and Op C–S–H as having Mg = 0.

TABLE V Percentage of TEM C–S–H analyses with Ca:Si atom ratio > 2

All C–S–H	Outer C–S–H	Inner C–S–H
12	4	19

2. With reference to Table V, it was decided that a cut-off excluding analyses with a Ca:Si atom ratio > 2 was a reasonable compromise between excluding too many Ip C–S–H analyses and including mixtures of Op C–S–H and $Ca(OH)_2$.

3. The upper limit for (Al + Fe):Ca ratio was simply derived by applying criteria 1 and 2.

The criteria appeared to include all the regions expected on visual examination to be inner product. The sulphur-rich analyses were always associated with high aluminium, but other aluminium-rich analyses existed. The former were concentrated in a few groups around the edges of the region, which were associated with similar analyses in the near-interface Op C–S–H and may well correspond to the inclusion of AFt crystals in the analysis volume as observed by TEM. The latter mostly occupied other near-interface positions although some were evident in the body of the region. These may be associated with small C_4AH_x-type or magnesium, aluminium-rich precipitates which have been observed by TEM in the inner product. Iron was present throughout the region, but did not appear to be particularly associated with either aluminium or sulphur. Iron also occurred in some of the areas high in sulphur.

The mean X:Ca ratios for each element, and the Ca:Si ratio, for both Ip and Op C–S–H analyses are given in Tables VI and VII. The Ca:Si ratio is higher in the outer product, as are the Al:Ca and S:Ca ratios. The Fe:Ca ratio is the same for both C–S–H gels. The alkalis sodium and potassium, are present only as trace elements, probably deposited from the pore solution during drying. Magnesium is, by definition, only in the IP C–S–H. Titanium and manganese are essentially absent.

The inner and outer product data were sorted into the classes used for the TEM data to facilitate comparison. Fig. 13a shows the variation in Al:Ca, Fe:Ca, S:Ca and Mg:Ca atom ratios with Ca:Si atom ratio (i.e. with the classes in the histograms), for the Ip C–S–H, and Fig. 13b shows the same for the Op C–S–H, with the obvious exception of magnesium. The elemental variations in both figures indicate the presence of second and third phases intimately mixed with the C–S–H gels. The implication is that the Ca:Si ratio of a class is not necessarily a true represention of the single-phase C–S–H present in the contributory analysis volumes. This is outlined in the following example.

If it was assumed that the class with mean Ca:Si = 1.67 was composed entirely of single-phase C–S–H, that all other elements were present as substituents within this gel, and that the underlying Al:Ca ratio decreases with increasing Ca:Si according to the trend found in the TEM results above, such that the C–S–H with Ca:Si = 1.67 has Al:Ca = 0.028 and the C–S–H with Ca:Si = 1.725 has Al:Ca = 0.027, then it is evident from Fig. 13a that the value of Al:Ca = 0.034 observed at Ca:Si = 1.725 can only be achieved through the involvement of a high aluminium-bearing phase. As the Mg:Ca ratio does not increase significantly between these two adjacent classes (Ca:Si = 1.67 and 1.725), the TEM evidence indicates that the phase intermixed with the C–S–H must be a calcium sulphoaluminate hydrate. As the S:Ca and Fe:Ca ratios also do not increase significantly, the best option is a sulphur-deficient low-iron AFm-type phase, i.e. C_4AH_x. If this phase were only intermixed with the two C–S–H gels outlined above, then the Al:Ca ratio observed in the Ca:Si = 1.725 class, could be achieved by the proportions indicated in Table VIII. Further increases in mean Ca:Si ratio are accompanied by an increase in S:Ca ratio, which suggests the presence of small amounts of high sulphur-bearing phases, either monosulphate or AFt. Clearly, this is simplistic, and in reality C–S–H gels with a range of Ca:Si ratios are probably intermixed with varying proportions of second and third phases, but it serves to demonstrate the probability of phase admixture within the analysis volumes. The same type of approach can be made to the Op C–S–H data on Fig. 13b, where again the influence of phase admixture is superimposed over the underlying trend of the Al:Ca ratio decreasing with increasing Ca:Si ratio.

Although it is apparent that the initial criteria for determining the compositional limits for single-phase

TABLE VI X:Ca atom ratios of inner product C–S–H in OPC determined by EMPA mapping, $n = 606$

Element	Mean ± σ	High	Low
Na	0.0013 ± 0.0016	0.0098	0.0000
Mg	0.0221 ± 0.0137	0.1327	0.0002
Al	0.0335 ± 0.0190	0.1062	0.0000
Si	0.6098 ± 0.0502	0.7517	0.5028
S	0.0109 ± 0.0142	0.0722	0.0000
K	0.0043 ± 0.0053	0.0300	0.0000
Ti	0.0003 ± 0.0012	0.0143	0.0000
Mn	0.0002 ± 0.0021	0.0469	0.0000
Fe	0.0156 ± 0.0055	0.0510	0.0045
Ca:Si	1.6513 ± 0.1378	1.9889	1.3303

TABLE VII X:Ca atom ratios of outer product C–S–H in OPC determined by EMPA mapping, $n = 161$

Element	Mean ± σ	High	Low
Na	0.0020 ± 0.0020	0.0070	0.0000
Mg	0.0000[a] –	–	–
Al	0.0509 ± 0.0200	0.1047	0.0072
Si	0.5636 ± 0.0403	0.7126	0.5017
S	0.0318 ± 0.0148	0.0681	0.0000
K	0.0086 ± 0.0070	0.0308	0.0000
Ti	0.0003 ± 0.0012	0.0127	0.0000
Mn	0.0001 ± 0.0004	0.0041	0.0000
Fe	0.0153 ± 0.0056	0.0306	0.0050
Ca:Si	1.7830 ± 0.1231	1.9933	1.4034

[a] By definition

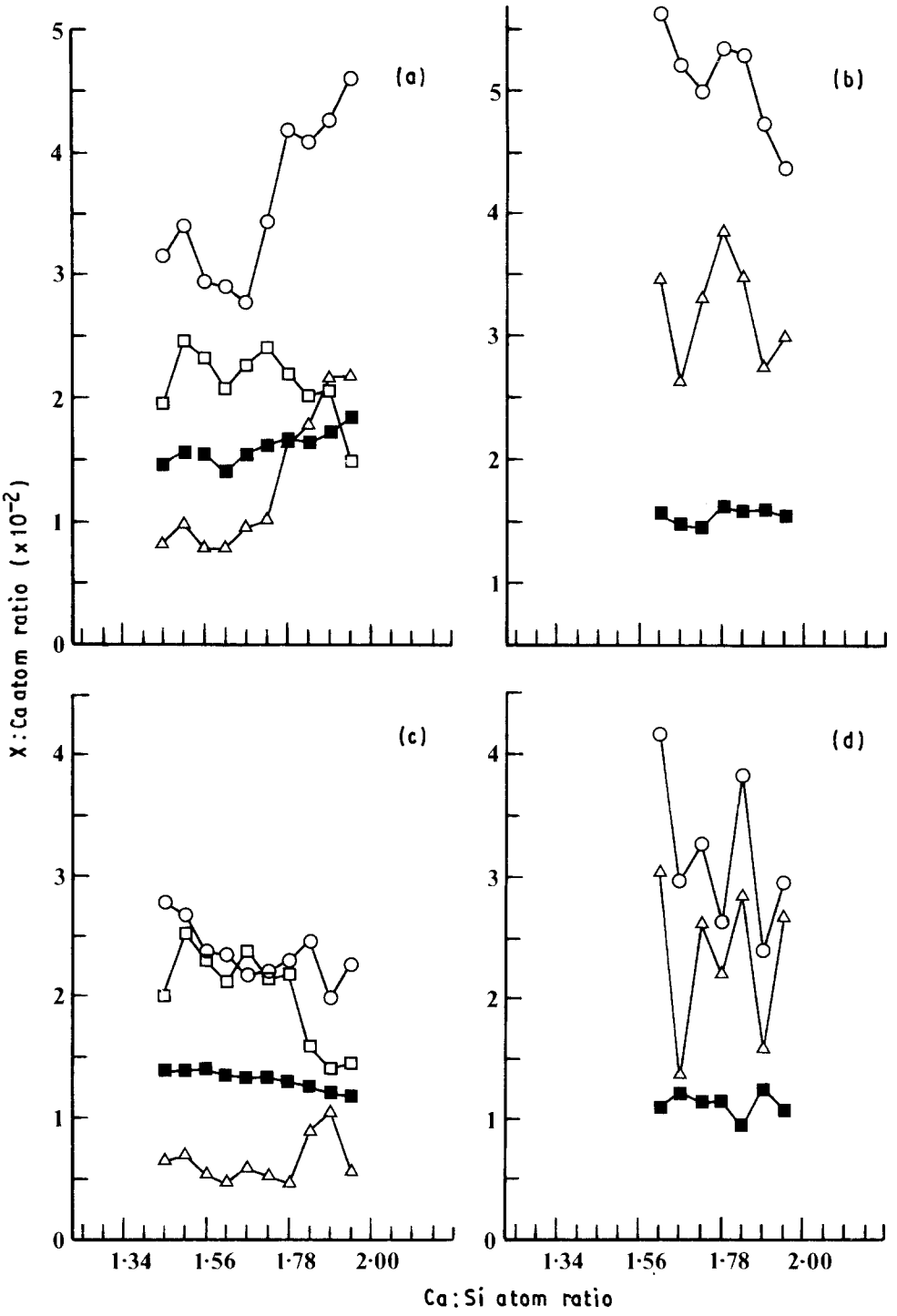

Figure 13 Variation in mean (○) Al:Ca, (■) Fe:Ca, (△) S:Ca and (□) Mg:Ca atom ratios with mean Ca:Si ratio for (a) inner and (b) outer product using the initial criteria, and (c) inner and (d) outer product using the restricted criteria.

C–S–H are consistent with TEM observations and the EMPA elemental maps, it is constructive in terms of determining the scale and extent of phase intermixing, to examine the effect of reducing the upper limit of (Al + Fe):Ca atom ratio by excluding all the near-interface inner product regions which were associated with higher aluminium and sulphur than the body of the inner product. In achieving this, 70% of analyses originally designated as Op C–S–H are excluded by the same criterion, leaving only 50 points considered as single-phase Op C–S–H (out of a total of 2500 analyses within the mapped area; the choice of area resulted in a roughly equal split between inner and outer product regions). The depleted statistics for Op C–S–H resulted in a distribution comparable to many of those produced by the TEM data, i.e. bimodal.

Fig. 13c shows the variation in Al:Ca, Fe:Ca, S:Ca and Mg:Ca atom ratios with the mean Ca:Si atom ratio classes for the restricted data for the Ip C–S–H (classified as before), and Fig. 13d shows the same for the Op C–S–H, with the exception of magnesium. For Ip C–S–H, it is evident that most of the analyses requiring the presence of second phases have been removed, revealing the underlying compositional trends, but also that some remain in what is only around two-thirds of the inner product region. The

TABLE VIII An example of the compositional effect of mixing two C–S–H gels of different compositions with an AFm phase (see text)

Fraction	Phase
0.4289	$C_{1.67}\ S\ A_{0.0234}\ H_x$
0.5652	$C_{1.725}\ S\ A_{0.0233}\ H_y$
0.0059	$C_4\ A\ H_z$
1.0000	

graph for the Op C–S–H involves only poor statistics, and this must be considered in any assessment; however, it is significant that the variation in Al:Ca ratio is mirrored by that of the S:Ca ratio. This suggests that even after restricting the compositional limits to levels which drastically reduce the number of analyses that may be considered as Op C–S–H, some analyses remain which require the presence of second phases within the X-ray generation volume. The implication is that single-phase Op C–S–H rarely occurs in this mature hardened OPC paste in volumes greater than $\approx 2\ \mu m^3$.

3.2.3. Composition of the AFt phase

Fig. 14 is a plot of (Al + Fe):Ca against S:Ca atom ratio for TEM analyses of AFt relicts from all the OPC pastes. The trend is towards the ideal composition for AFt of (Al + Fe):Ca = 0.33 and S:Ca = 0.50. Considering the damaged state of the AFt relicts, this is an excellent agreement with composition of ettringite and excludes the requirement to include silicon substitution which has been found necessary in previous studies [4, 7, 21]. As expected from the TEM analyses of single-phase C–S–H, the line-of-best-fit does not pass through the origin, but corresponds at S:Ca = 0, to (Al + Fe):Ca of between 0.03 and 0.05.

Only about 30% of the analyses had a detectable iron-content, and any underlying Fe:Ca is $\ll 0.01$. If the C–S–H is assumed to have zero iron, then the compositions of the AFt relicts range between $C_3\ (A_{0.91}\ F_{0.09})\ 3C\ \bar{S} \cdot H_x$ and $C_3\ (A_{0.59}\ F_{0.41})\ 3C\ \bar{S} \cdot H_x$. The average composition of the analyses involving iron is $C_3\ (A_{0.75}\ F_{0.25})\ 3C\ \bar{S} \cdot H_x$. As only 30% of total analyses detected iron, the average of all the analyses is $C_3\ (A_{0.925}\ F_{0.075})\ 3C\ \bar{S} \cdot H_x$ and $C_3\ (A_{1-y}\ F_y)\ 3C\ \bar{S} \cdot H_x$ where $0 < y < 0.41$.

3.2.4. Composition of AFm-type phases

Large crystals of AFm-type phases were observed in all the hardened pastes examined, from 1 day–$3\frac{1}{2}$ years, and although only a limited number of analyses were taken, there did not appear to be any relationship between compostion and age. The crystals analysed had compositions within the range $C_3\ (A_{1-x}\ F_x) \cdot C\ (\bar{S}_y\ H_{1-y}) \cdot H_z$, where $0 < y < 0.15$ by TEM, or $0 < y < 0.08$ by EMPA, $0 < x < 0.31$ by TEM, or $0 < x < 0.36$ by EMPA.

For the AFt, there was no requirement to incorporate silicon into the formula, as found necessary by Harrisson *et al.* [3]. The (Al + Fe):Ca atom ratio never deviated far from the theoretical value of 0.5, so there was no need to postulate the presence of hydroxoaluminate in interlayer sites, as found necessary by Lachowski *et al.* [4] and Taylor *et al.* [7].

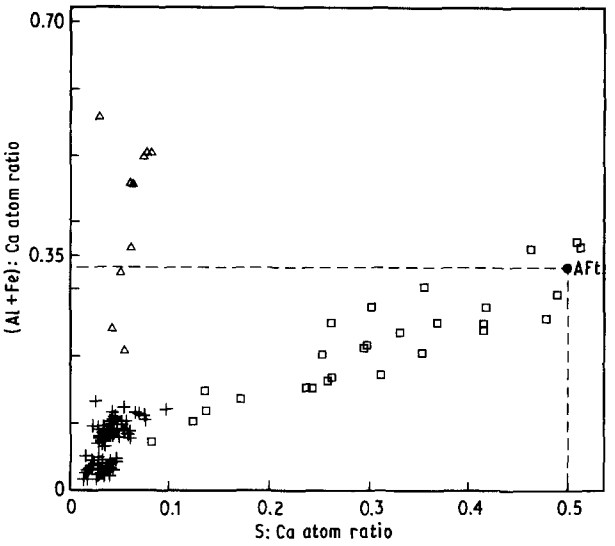

Figure 14 Plot of (Al + Fe):Ca against S:Ca atom ratio for TEM analyses of (□) AFt relicts, (△) AFm and (+) C–S–H for OPC samples of all ages (24 h–$3\frac{1}{2}$ years).

4. Conclusions

1. Inner and outer product C–S–H differ in morphology but not substantially in Ca:Si ratio.
2. TEM analysis indicates no systematic variation in C–S–H composition with age but significant variation from one area to another. There is some indication of a bimodal distribution of Ca:Si ratios at early ages which subsequently disappears.
3. TEM microanalysis of AFt relicts shows them to have (Al + Fe):Ca and S:Ca ratios of ettringite.
4. Inner product C–S–H occasionally contains embedded within it small amounts of AFt, AFm, a magnesium-rich phase and $Ca(OH)_2$. The possible presence of these phases must be considered when interpreting microprobe analyses of inner product.
5. Microanalysis by EMPA gives Ca:Si ratios in substantial agreement with those found by TEM, but it is shown that it is essentially impossible to obtain by EMPA analyses of single-phase Op C–S–H without admixture of other phases, particularly sulphoaluminate phases. Despite the presence of small amounts of embedded phases as revealed by TEM, single-phase Ip C–S–H can be analysed by EMPA.

Acknowledgements

Thanks are due to SERC for financial support (IGR) and to C. R. Wilding, Harwell Laboratory, for the supply of material and helpful discussions.

References

1. D. L. RAYMENT and A. J. MAJUMDAR, *Cem. Conc. Res.* **12** (1982) 753.
2. H. F. W. TAYLOR and D. E. NEWBURY, *ibid.* **14** (1984) 565.
3. A. M. HARRISSON, N. B. WINTER and H. F. W. TAYLOR, in "Proceedings of the 8th International Congress

on the Chemistry of Cement", Vol. 4 (FINEP, Rio de Janeiro, 1986) p. 170.
4. E. E. LACHOWSKI, K. MOHAN, H. F. W. TAYLOR and A. E. MOORE, *J. Amer. Ceram. Soc.* **63** (1980) 447.
5. E. E. LACHOWSKI, K. MOHAN, H. F. W. TAYLOR, C. D. LAWRENCE and A. E. MOORE, *ibid.* **64** (1981) 319.
6. E. E. LACHOWSKI and S. DIAMOND, *Cem. Conc. Res.* **13** (1983) 177.
7. H. F. W. TAYLOR, K. MOHAN and G. K. MOIR, *J. Amer. Ceram. Soc.* **68** (1985) 680.
8. G. W. GROVES, P. J. LE SUEUR and W. SINCLAIR, *ibid.* **69** (1986) 353.
9. G. W. GROVES, *Mater. Res. Soc. Symp. Proc.* **85** (1987) 3.
10. G. W. GROVES and S. A. RODGER, *Adv. Cem. Res.* **2** (1989) 135.
11. S. A. RODGER and G. W. GROVES, *J. Amer. Ceram. Soc.* **72** (1989) 1037.
12. H. F. W. TAYLOR, in "Cement chemistry" (Academic Press, London, 1990).
13. G. CLIFF and G. W. LORIMER, *J. Microsc.* **103** (1975) 203.
14. B. J. DALGLEISH and K. IBE, *Cem. Conc. Res.* **11** (1981) 729.
15. B. J. DALGLEISH, A. GHOSE, H. M. JENNINGS and P. L. PRATT, in "Proceedings of the 11th International Conference on the Science of Ceramics", Vol. 2 edited by R. Carlsson and S. Karlsson (Swedish Ceramic Society, Stockholm, 1981) p. 297.
16. I. G. RICHARDSON, G. W. GROVES and S. A. RODGER, *Mater. Res. Soc. Symp. Proc.* **137** (1989) 313.
17. D. L. RAYMENT and E. E. LACHOWSKI, *Cem. Conc. Res.* **14** (1984) 43.
18. H. F. W. TAYLOR, *J. Amer. Ceram. Soc.* **69** (1986) 464.
19. I. G. RICHARDSON and G. W. GROVES, *Cem. Conc. Res.* (1992).
20. *Idem, J. Mater. Sci.* (1991).
21. S. DIAMOND and E. E. LACHOWSKI, *Cem. Conc. Res.* **13** (1983) 335.

Received 15 October 1991
and accepted 29 January 1992